Differentiating gastric cancer and gastric lymphoma using texture analysis (TA) of positron emission tomography (PET)

Yi-Wen Sun[1], Chang-Feng Ji[2], Han Wang[2], Jian He[2], Song Liu[2], Yun Ge[3], Zheng-Yang Zhou[1]

[1]Department of Nuclear Medicine, Nanjing Drum Tower Hospital Clinical College of Nanjing Medical University, Nanjing, Jiangsu 210008, China;
[2]Department of Radiology, Nanjing Drum Tower Hospital Clinical College of Nanjing Medical University, Nanjing, Jiangsu 210008, China;
[3]School of Electronic Science and Engineering, Nanjing University, Nanjing, Jiangsu 210093, China.

Abstract

Background: Texture analysis (TA) can quantify intra-tumor heterogeneity using standard medical images. The present study aimed to assess the application of positron emission tomography (PET) TA in the differential diagnosis of gastric cancer and gastric lymphoma.

Methods: The pre-treatment PET images of 79 patients (45 gastric cancer, 34 gastric lymphoma) between January 2013 and February 2018 were retrospectively reviewed. Standard uptake values (SUVs), first-order texture features, and second-order texture features of the grey-level co-occurrence matrix (GLCM) were analyzed. The differences in features among different groups were analyzed by the two-way Mann-Whitney test, and receiver operating characteristic (ROC) analysis was used to estimate the diagnostic efficacy.

Results: $\text{Inertia}_{\text{GLCM}}$ was significantly lower in gastric cancer than that in gastric lymphoma (4975.61 *vs.* 11,425.30, $z = -3.238$, $P = 0.001$), and it was found to be the most discriminating texture feature in differentiating gastric lymphoma and gastric cancer. The area under the curve (AUC) of $\text{inertia}_{\text{GLCM}}$ was higher than the AUCs of SUVmax and SUVmean (0.714 *vs.* 0.649 and 0.666, respectively). SUVmax and SUVmean were significantly lower in low-grade gastric lymphoma than those in high grade gastric lymphoma (3.30 *vs.* 11.80, 2.40 *vs.* 7.50, $z = -2.792$ and -3.007, $P = 0.005$ and 0.003, respectively). SUVs and first-order grey-level intensity features were not significantly different between low-grade gastric lymphoma and gastric cancer. $\text{Entropy}_{\text{GLCM12}}$ was significantly lower in low-grade gastric lymphoma than that in gastric cancer (6.95 *vs.* 9.14, $z = -2.542$, $P = 0.011$) and had an AUC of 0.770 in the ROC analysis of differentiating low-grade gastric lymphoma and gastric cancer.

Conclusions: $\text{Inertia}_{\text{GLCM}}$ and $\text{entropy}_{\text{GLCM}}$ were the most discriminating features in differentiating gastric lymphoma from gastric cancer and low-grade gastric lymphoma from gastric cancer, respectively. PET TA can improve the differential diagnosis of gastric neoplasms, especially in tumors with similar degrees of fluorodeoxyglucose uptake.

Keywords: Image processing; Computer-assisted; Stomach neoplasms; Lymphoma; Fluorodeoxyglucose F18; Positron emission computed tomography

Introduction

Gastric cancer is a common malignancy and a major cause of cancer-related death globally.[1] Gastric lymphoma is the most common extranodal lymphoma.[2] Despite the similarities in clinical and radiological features, the treatment strategies and clinical outcomes highly differ between gastric cancer and gastric lymphoma.[3-6] Therefore, the importance of differentiating gastric cancer from gastric lymphoma has been highlighted.

Although endoscopic biopsy is a solid differential method, it is an invasive procedure with sampling limitations, and it can hardly assess lesions outside the submucosal layer.[7,8] On the other hand, non-invasive imaging modalities can simultaneously display the entire lesion and its adjacent structures. Contrast-enhanced multidetector-row computed tomography (CT) can reflect the blood supply, capillary density, and dysfunctional neo-vessels of gastric tumors, and is presently the most widely used imaging technique for gastric tumors.[9,10] However, the use of CT in differentiating gastric cancer from gastric lymphoma based on features such as lesion distribution, wall thickness, and enhancement pattern remains controversial.[11] Magnetic resonance imaging (MRI) has been increasingly used because of its excellent soft-tissue resolution. Although diffusion-weighted imaging of

Access this article online

Quick Response Code:

Website: www.cmj.org

DOI: 10.1097/CM9.0000000000001206

Yi-Wen Sun and Chang-Feng Ji contributed equally to this work.

Correspondence to: Dr. Zheng-Yang Zhou, Department of Nuclear Medicine, Nanjing Drum Tower Hospital Clinical College of Nanjing Medical University, No. 321 Zhongshan Road, Nanjing, Jiangsu 210008, China
E-Mail: zyzhou@nju.edu.cn

Copyright © 2021 The Chinese Medical Association, produced by Wolters Kluwer, Inc. under the CC-BY-NC-ND license. This is an open access article distributed under the terms of the Creative Commons Attribution-Non Commercial-No Derivatives License 4.0 (CCBY-NC-ND), where it is permissible to download and share the work provided it is properly cited. The work cannot be changed in any way or used commercially without permission from the journal.

Chinese Medical Journal 2021;134(4)
Received: 26-05-2020 **Edited by:** Peng Lyu

MRI, which reflects the mobility of water protons in biological tissues,[12] has been reported to exhibit a higher apparent diffusion coefficient in gastric lymphoma, than that in gastric cancer,[13] it has the disadvantages of artifacts and a long scanning time, and the application of MRI in gastric lymphoma is limited. ^{18}F-fluorodeoxyglucose (FDG) positron emission tomography (PET) can visibly and comprehensively assess the glucose metabolism of tissues and has been widely used in a variety of malignant tumors including gastric cancer and lymphoma.[14-16] Semi-quantitatively, the standard uptake value (SUV) and its derivatives, which correlate to the degree of FDG uptake in tissues, have been demonstrated to help differentiate gastric cancer from gastric lymphoma.[17,18] Nonetheless, FDG uptake has a wide range in both gastric cancer and gastric lymphoma,[15,17,19] which is partially due to the differences between pathological subtypes. Therefore, the differential diagnostic accuracy based on only SUV and its derivatives is moderate.

Texture analysis (TA) refers to a variety of mathematical methods that describe the frequency distribution of the grey-level intensities of pixels or voxels, and the spatial relationship between them.[20-22] As a technique to quantitively estimate intra-tumor heterogeneity, TA can extract numerous features from standard clinical images, providing additional information beyond visual interpretation.[23] In gastric lesions, CT texture features have exhibited potential in assisting in the differential diagnosis, assessing histopathological characteristics, evaluating the therapeutic response, and predicting clinical outcomes.[10,24,25] However, CT TA only presents variability in tissue density, which may have resulted from diversified cellularity, necrosis, vascularization, or perfusion. In contrast, since ^{18}F-FDG PET is a metabolic imaging modality, its TA conveys the spatially varying distribution of ^{18}F-FDG uptake, which is associated with cellular and molecular characteristics such as cell proliferation, glucose transporter expression, and hexokinase activity.[20] Previous studies have shown that PET TA can be a useful tool for the diagnosis, staging, response predicting, and prognosis in a variety of tumors.[20,26,27] However, to the best of our knowledge, limited studies have reported the applications of PET TA in improving the differential diagnosis of gastric cancer and gastric lymphoma.

Therefore, the present study retrospectively analyzed the texture features derived from standard PET images of gastric cancer and gastric lymphoma to explore the role of PET TA in the differential diagnosis.

Methods

Ethics

The present study was approved by the Ethics Committee of Nanjing Drum Tower Hospital (No. 2018-143-01). As a retrospective and anonymous study, the requirement for informed consent was waived.

Patient selection

The data of 106 patients clinically diagnosed with gastric carcinoma or gastric lymphoma from January 2013 to February 2018 were gathered and reviewed. The inclusion criteria were as follows: (1) a diagnosis of gastric carcinoma or gastric lymphoma confirmed by gastroscopic biopsy or surgical pathology, and (2) ^{18}F-FDG PET/CT scan before treatment. The exclusion criteria were as follows: (1) past cancer history ($n = 8$), (2) any local or systemic treatment before the PET/CT scan ($n = 1$), (3) incomplete clinical or pathological data ($n = 9$), (4) the interval between the scan and biopsy or surgery was longer than 2 weeks ($n = 1$), and (5) no observable FDG uptake in the lesions ($n = 8$). The flowchart for study enrollment is presented in Figure 1.

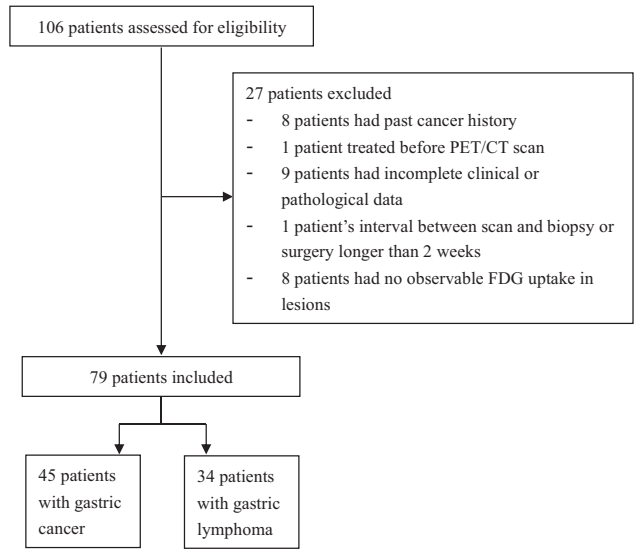

Figure 1: Flowchart of study enrollment shows the ultimate inclusion of 79 patients (45 with gastric cancer and 34 with gastric lymphoma). PET/CT: Positron emission tomography/computed tomography; FDG: Fluorodeoxyglucose.

^{18}F-FDG PET/CT image acquisition

All patients were requested to fast for at least 6 h before tracer injection with a serum glucose level of <11.1 mmol/L. ^{18}F-FDG (JYAMS PET Research and Development Limited, Nanjing, Jiangsu, China) was intravenously injected at a dose of 5.2 MBq (±10%) per kilogram of body weight. After sitting still for 50 to 90 min, the patients were instructed to drink 600 to 1000 mL of water to achieve gastric distension and were scanned in the supine position with breathing at rest.

The ^{18}F-FDG PET/CT scans were performed using a 16-slice hybrid PET/CT scanner (Gemini GXL16, Philips Medical System, Cleveland, OH, USA). An unenhanced CT scan from the skull base to the upper thigh was performed for attenuation correction (CT scanning parameters: 50 mA, 120 kV, 5 mm section thickness, 5 mm increment, and a pitch of 0.813). A three-dimensional PET scan of the same region was subsequently acquired (8–9 fields of view, 70 s per field). Then, the PET images were reconstructed in a 144 × 144 matrix with a voxel size of 4 mm × 4 mm × 4 mm and a slice thickness of 4 mm by a line-of-response algorithm. CT images were

reconstructed to a 512 × 512 matrix with a pixel size of 1.17 mm × 1.17 mm. The attenuation-corrected PET/CT fusion images on three orthogonal (transaxial, coronal, and sagittal) planes were reviewed.

SUV measurement and TA

All ^{18}F-FDG PET/CT images were transferred to a MedEx workstation (MedEx Technology Limited Corporation, Beijing, China) and retrospectively interpreted by one experienced radiologist (Y.S. with 9 years of experience in oncologic PET/CT) who was blinded to the histological results. To avoid the effect of FDG uptake in the normal gastric wall, the abnormalities on the CT images and the tumor location confirmed by gastroscopy or surgical specimens were reviewed. The gastric lesions presented as abnormal FDG-avid foci were analyzed. After enclosing each tumor in a cropping sphere, the MedEx workstation automatically generated the SUVmax and SUVmean using the threshold of 0.4 × SUVmax as the border of the tumor.

To proceed with the TA, the PET and CT images were downloaded from the MedEx workshop and uploaded into the in-house software Image Analyzer 2.0 (School of Electronic Science and Engineering, Nanjing University, Nanjing, Jiangsu, China). The regions of interest (ROIs) were manually drawn slice by slice to cover the entire volume of the gastric lesions on the standard PET images, referring to the hybrid low-dose CT images. The gastric lumen and any metastatic lesions (metastatic lymph node, hepatic metastasis, etc) close to the primary tumors were carefully avoided. The ROIs were drawn by the same radiologist after three months to evaluate the intra-observer agreement and by another radiologist (S.L. with 8 years of experience in gastroenterology imaging) to estimate the interobserver agreement. After drawing all the ROIs, the software automatically read the grey-level intensity of each pixel within the ROIs, and generated a set of texture features, as follows: (1) histogram features: mean, standard deviation (SD), max-frequency, mode, minimum, maximum, cumulative percentiles (the 5th, 10th, 25th, 50th, 75th, and 90th percentile), skewness, kurtosis, entropy, volume, area, and max-diameter; and (2) local textural features of the grey-level co-occurrence matrix (GLCM): $entropy_{GLCM}$ and $inertia_{GLCM}$ (The $entropy_{GLCM}$ was defined by the formular $Entropy_{GL}$= $-\sum i\sum jG(i,j)\log G(i,j)$. It describes the randomness of grey-level intensities of pairs of pixels, the more chaotically the intensities of pairs of pixels distributed, the higher the $entropy_{GLCM}$ will be. $Inertia_{GLCM}$ was defined by the formular $Inertia_{GLCM}= \sum i\sum j(i-j)^2G(i,j)$. It describes the local variation between a pixel and its neighbors, the more the grey-level intensities vary from pixels to their neighbors, the higher the $inertia_{GLCM}$ will be).

Statistical analysis

The normality of the data was analyzed using the Kolmogorov-Smirnov test. The two-way Mann-Whitney test was used to compare the differences in SUVs and texture features between gastric cancer *vs.* gastric lymphoma, low-grade *vs.* high-grade gastric lymphoma, and low-grade gastric lymphoma *vs.* gastric cancer. The correlations among SUVmax, SUVmean, and histogram parameters were assessed by Spearman correlation test. The differential efficacy of the SUVmax, SUVmean, and texture parameters in different types of gastric neoplasms was evaluated through receiver operating characteristic (ROC) analysis, and the areas under the curves (AUCs) were compared by *z*-test. The intra-observer and inter-observer agreement in the measurement of the PET texture features was estimated by intra-class correlation coefficients (ICCs; 0–0.200, poor; 0.201–0.400, fair; 0.301–0.600, moderate; 0.601–0.800, good; 0.801–1.000, excellent). The ROC analysis was performed using Med-Calc Statistical Software version 19.0.7 (Med-Calc Software bvba, Ostend, Belgium). Other statistical analyses were performed using SPSS version 22.0 (IBM SPSS, Chicago, IL, USA). A two-tailed *P* value of <0.05 was considered statistically significant.

Results

Patient characteristics

A total of 79 patients (47 males and 32 females; age range: 23–88 years; median age: 60 years) served as our study cohort, including 45 in the gastric carcinoma group and 34 in the gastric lymphoma group. The clinical and pathological characteristics are displayed in Table 1.

Table 1: Clinical and pathological characteristics of patients with gastric cancer and gastric lymphoma included (*n* = 79).

Characteristics	Gastric carcinoma (*n* = 45)	Gastric lymphoma (*n* = 34)
Gender		
Male	32	15
Female	13	19
Age		
<60 years	18	21
≥60 years	27	13
Location		
Cardia and fundus	15	4
Body	20	22
Antrum	10	8
Histological type		
Adenocarcinoma	32	–
Signet-ring cell carcinoma	9	–
Neuroendocrine carcinoma	3	–
Undifferentiated carcinoma	1	–
MALT lmphoma	–	8
Diffuse large B cell lmphoma	–	21
High-grade B cell lmphoma	–	3
Low-grade B cell lmphoma	–	1
Peripheral T cell lymphoma	–	1
Histopathology access		
Gastroscopic biopsy	35	34
Surgery	10	0

Data are presented as *n*. MALT: Mucosa associated lymphoid tissue; –: Not aplicable.

Table 2: Differences of SUVs and texture features between gastric cancer and gastric lymphoma.

Parameters	Gastric cancer	Gastric lymphoma	*z*	*P*
Mean	2218.99 (921.79–3416.51)	2999.42 (1628.44–5861.95)	−2.277	0.023
SD	350.14 (168.68–876.44)	624.21 (279.75–2212.96)	−2.277	0.023
Max-frequency	4.00 (3.00–5.00)	4.00 (2.00–4.00)	−0.764	0.445
Mode	1774.00 (886.00–2661.00)	2002.00 (1347.75–4014.25)	−1.698	0.089
Minimum	1010.00 (541.00–1773.00)	1449.50 (893.00–2001.00)	−2.104	0.035
Maximum	3246.00 (1405.00–6360.50)	5333.50 (2309.00–12,873.75)	−2.188	0.029
5th percentile	1430.00 (653.50–2376.50)	1737.50 (1196.25–3023.75)	−1.901	0.057
10th percentile	1546.00 (711.50–2479.50)	1909.50 (1267.25–3291.00)	−2.030	0.042
25th percentile	1720.00 (792.50–2742.50)	2236.00 (1386.50–3893.25)	−2.099	0.036
50th percentile	2063.00 (935.00–3225.00)	2869.50 (1627.50–5400.00)	−2.188	0.029
75th percentile	2437.00 (1046.00–3845.00)	3347.00 (1730.50–7341.75)	−2.297	0.022
90th percentile	2838.00 (1123.00–4397.00)	3923.50 (1797.25–9056.50)	−2.248	0.025
Skewness	0.48 (0.07–0.92)	0.47 (0.16–0.82)	−0.069	0.945
Kurtosis	3.05 (2.60–3.91)	2.78 (2.38–3.26)	−1.852	0.064
$Entropy_{HIST}$	5.73 (4.72–6.63)	5.70 (4.72–7.13)	−0.584	0.559
Volume	29,632.00 (9920.00–72,032.00)	19,552.00 (9184.00–95,584.00)	−0.223	0.824
Area	7408.00 (2480.00–18,008.00)	4888.00 (2296.00–23,893.00)	−0.223	0.824
Max-diameter	60.22 (35.93–78.18)	46.36 (32.98–79.79)	−0.446	0.656
$Entropy_{GLCM10}$	9.00 (7.30–10.15)	7.61 (7.11–10.12)	−1.074	0.283
$Entropy_{GLCM11}$	9.33 (7.60–10.28)	7.90 (7.25–10.25)	−1.129	0.259
$Entropy_{GLCM12}$	9.14 (7.34–10.11)	7.71 (6.71–10.16)	−1.069	0.285
$Entropy_{GLCM13}$	9.26 (7.59–10.25)	8.04 (7.31–10.34)	−0.970	0.332
$Inertia_{GLCM10}$	6020.79 (1700.47–16,367.30)	19,602.65 (4466.55–40,418.13)	−2.921	0.003
$Inertia_{GLCM11}$	4975.61 (747.88–8615.51)	11,425.30 (4415.08–26,092.18)	−3.238	0.001
$Inertia_{GLCM12}$	8179.52 (1291.79–20,038.60)	21,663.40 (7375.84–28,800.30)	−2.842	0.004
$Inertia_{GLCM13}$	3761.54 (585.62–10,314.60)	13,716.45 (2627.29–18,225.03)	−2.842	0.004
SUVmax	4.90 (3.05–9.80)	9.40 (3.60–19.50)	−2.258	0.024
SUVmean	3.10 (2.10–5.85)	5.75 (2.63–12.00)	−2.516	0.012

Data are presented as median (interquartile range). SUV: Standard uptake value; SD: Standard deviation; HIST: Histogram; GLCM: Grey-level co-occurrence matrix.

Difference between gastric cancer and gastric lymphoma

The SUVs and some texture features did not comply with the normal distribution. Thus, the two-way Mann-Whitney test was used to compare the differences in SUVs and texture features among the groups.

There were significant differences in terms of SUVmax, SUVmean, maximum, mean, SD, minimum, percentiles (10th, 25th, 50th, 75th, and 90th), and $inertia_{GLCM10\text{-}13}$ ($P = 0.001$–0.042) between the gastric cancer group and the gastric lymphoma group [Table 2]. Representative images of gastric cancer and gastric lymphoma are presented in Figure 2. The max-frequency, mode, 5th percentile, skewness, kurtosis, entropy, volume, area, max diameter, and $entropy_{GLCM}$ were not significantly different between gastric cancer and gastric lymphoma.

Difference between low-grade and high-grade gastric lymphoma

There were nine low-grade gastric lymphoma cases (eight cases of mucosa-associated lymphoid tissue [MALT] lymphoma and one case of low-grade B cell lymphoma) and 25 high-grade gastric lymphoma cases (21 cases of diffuse large B cell lymphoma, three cases of high-grade B cell lymphoma, and one case of peripheral T cell lymphoma). SUVmax, SUVmean, SD, volume, area, max-diameter, and $entropy_{HIST}$ were significantly lower in low-grade gastric lymphoma than those in high-grade gastric lymphoma (the *z* value ranged from −3.007 to −2.01, the *P* value ranged from 0.003 to 0.044) [Table 3].

Difference between low-grade gastric lymphoma and gastric cancer

$Entropy_{GLCM10\text{-}13}$ was found to be significantly lower in low-grade lymphoma than that in gastric cancer (the *z* value ranged from −2.542 to −2.309, the *P* value ranged from 0.011 to 0.021). Volume and area were also found to be significantly lower in low-grade lymphoma than those in gastric cancer ($z = -2.066$ and −2.066, $P = 0.039$ and 0.039, respectively). However, there were no significant differences in the SUVs or other grey-level intensity features between low-grade gastric lymphoma and gastric cancer.

Correlations between SUVs and histogram features

The mean, SD, maximum, minimum, and percentiles (10th, 25th, 50th, 75th, and 90th) derived from the grey-level intensity histogram analysis showed significant positive correlations with SUVmax and SUVmean, with $P \leq 0.001$ [Table 4].

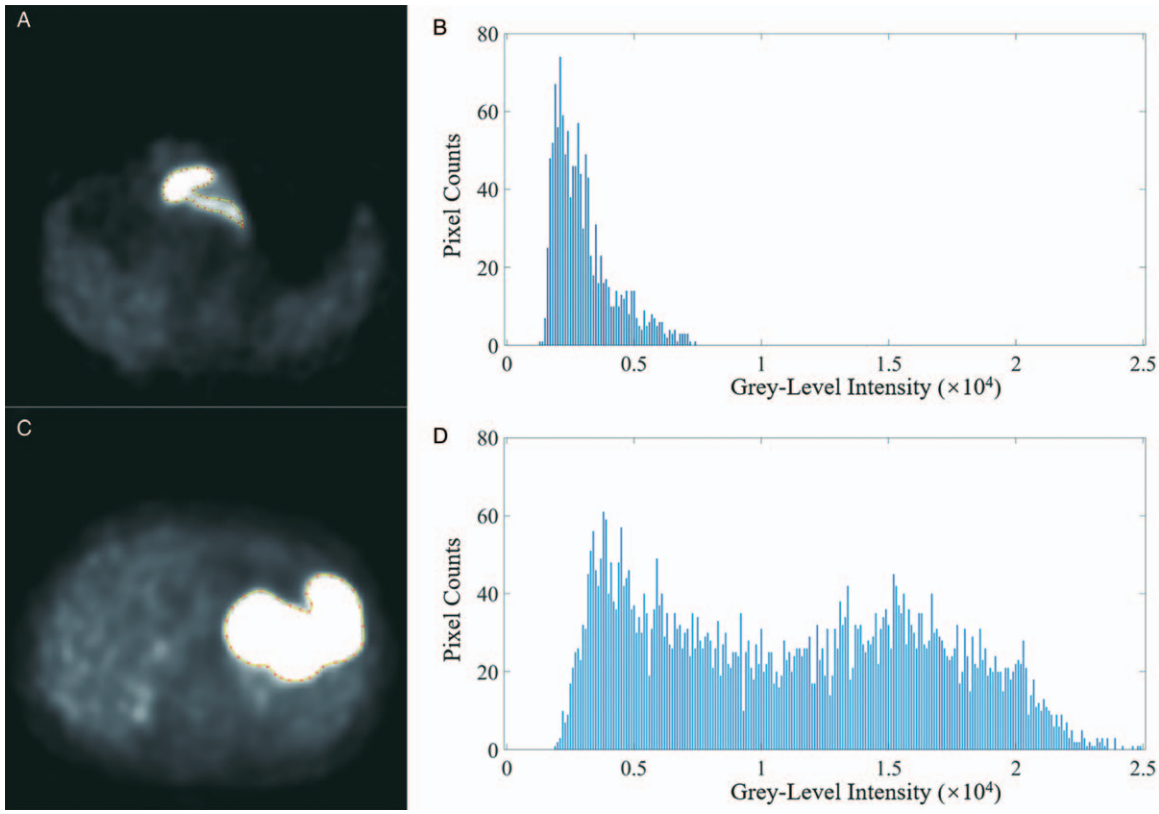

Figure 2: Axial positron emission tomography image (A) and grey-level intensity histogram (B) of an 84-year-old male with gastric adenocarcinoma. Axial PET image (C) and (D) grey-level intensity histogram of a 58-year-old woman with diffuse large B-cell lymphoma. PET: Positron emission tomography.

Table 3: Differences of SUVs and texture features between low-grade and high-grade gastric lymphoma.

Parameters	Low-grade gastric lymphoma	High-grade gastric lymphoma	*z*	*P*
Mean	2292.44 (1125.39–3599.91)	3349.84 (1788.23–7814.44)	−1.542	0.123
SD	285.14 (147.74–537.37)	1023.41 (344.54–3275.63)	−2.596	0.009
Max-frequency	4.00 (2.00–4.00)	4.00 (2.00–5.00)	−0.782	0.434
Mode	1919.00 (1073.00–3349.50)	2085.00 (1316.50–4428.00)	−0.644	0.520
Minimum	1283.00 (792.50–1916.5.00)	1533.00 (874.00–2085.00)	−0.527	0.598
Maximum	3265.00 (1574.00–5333.50)	6745.00 (2777.50–16,148.50)	−2.088	0.037
5th percentile	1715.00 (915.0–2217.50)	1760.0 (1207.00–3438.00)	−0.870	0.380
10th percentile	1872.00 (970.50–2401.00)	1919.00 (1291.50–3847.50)	−1.034	0.301
25th percentile	2101.00 (1017.5–2691.50)	2309.00 (1475.00–5063.50)	−1.152	0.250
50th percentile	2263.00 (1112.50–3405.50)	3367.00 (1746.00–7359.00)	−1.374	0.178
75th percentile	2466.00 (1201.5–4216.00)	4711.00 (1978.00–10,063.50)	−1.698	0.089
90th percentile	2601.00 (1335.500–4557.00)	3923.50 (2192.50–12,051.50)	−1.854	0.064
Skewness	0.38 (0.14–0.72)	0.55 (0.15–0.91)	−0.800	0.424
Kurtosis	2.90 (2.33–3.21)	2.76 (2.32–3.31)	−0.215	0.830
$Entropy_{HIST}$	4.49 (4.72–5.17)	6.17 (5.07–7.30)	−2.557	0.011
Volume	9088.00 (6496.00–13,696.00)	40,320.00 (11,680.00–146,976.00)	−2.518	0.012
Area	2272.00 (1624.00–3424.00)	10,080.00 (2920.00–36,744.00)	−2.518	0.012
Max-diameter	37.72 (27.24–52.25)	51.02 (36.02–89.06)	−2.010	0.044
$Entropy_{GLCM10}$	7.30 (5.97–7.93)	9.06 (7.16–10.30)	−1.854	0.064
$Entropy_{GLCM11}$	7.33 (6.43–8.02)	9.35 (7.34–10.45)	−2.049	0.040
$Entropy_{GLCM12}$	6.95 (5.60–7.93)	9.16 (7.13–10.33)	−2.128	0.033
$Entropy_{GLCM13}$	7.63 (6.25–8.09)	9.44 (7.44–10.50)	−1.854	0.064
$Inertia_{GLCM10}$	4484.86 (836.16–15,181.25)	23,842.40 (11,422.04–44,727.15)	−2.518	0.012
$Inertia_{GLCM11}$	5682.64 (948.69–12,101.45)	14,568.40 (6680.19–27,752.70)	−1.815	0.069
$Inertia_{GLCM12}$	22,103.70 (1505.08–36,206.75)	21,423.00 (9680.64–29,780.65)	−0.176	0.861
$Inertia_{GLCM13}$	6522.99 (400.27–20,267.20)	14,595.40 (3264.66–18,549.15)	−0.956	0.339
SUVmax	3.30 (2.75–4.45)	11.80 (6.85–21.75)	−2.792	0.005
SUVmean	2.40 (1.95–5.10)	7.50 (5.10–13.25)	−3.007	0.003

Data are presented as median (interquartile range). SUV: Standard uptake value; SD: Standard deviation; HIST: Histogram; GLCM: Grey-level co-occurrence matrix.

Table 4: Correlations between SUVs and grey-level intensity histogram features.

	SUVmax		SUVmean	
Parameters	Correlation coefficients	*P*	Correlation coefficients	*P*
Mean	0.643	<0.001	0.653	<0.001
SD	0.818	<0.001	0.802	<0.001
Minimum	0.369	0.001	0.401	<0.001
Maximum	0.760	<0.001	0.751	<0.001
10th percentile	0.479	<0.001	0.506	<0.001
25th percentile	0.520	<0.001	0.543	<0.001
50th percentile	0.603	<0.001	0.671	<0.001
75th percentile	0.680	<0.001	0.686	<0.001
90th percentile	0.718	<0.001	0.719	<0.001

SUV: Standard uptake value; SD: Standard deviation.

Table 5: ROC analysis of SUVs and texture parameters in differentiating gastric cancer *vs.* gastric lymphoma, low-grade gastric lymphoma *vs.* high grade gastric lymphoma and low-grade gastric lymphoma *vs.* gastric cancer.

Parameters	Cut-off	Sensitivity	Specificity	Accuracy	AUC	*P*
Gastric cancer *vs.* gastric lymphoma						
Mean	3687.22	0.822	0.471	0.671	0.650	0.018
SD	238.50	0.422	0.853	0.608	0.650	0.018
Minimum	1349.00	0.689	0.559	0.633	0.639	0.028
Maximum	1741.00	0.333	0.912	0.582	0.644	0.023
10th percentile	805.00	0.311	0.912	0.570	0.634	0.036
25th percentile	2056.00	0.622	0.618	0.620	0.639	0.029
50th percentile	3131.00	0.756	0.500	0.646	0.644	0.023
75th percentile	4581.00	0.844	0.441	0.671	0.652	0.017
90th percentile	6868.00	0.933	0.324	0.671	0.648	0.020
$Inertia_{GLCM10}$	13,232.50	0.733	0.618	0.684	0.693	0.002
$Inertia_{GLCM11}$	8625.99	0.778	0.647	0.722	0.714	<0.001
$Inertia_{GLCM12}$	20,258.70	0.800	0.529	0.684	0.688	0.002
$Inertia_{GLCM13}$	11,737.40	0.844	0.559	0.722	0.688	0.003
SUVmax	15.40	0.933	0.382	0.696	0.649	0.023
SUVmean	7.10	0.889	0.441	0.696	0.666	0.009
Low-grade gastric lymphoma *vs.* high grade gastric lymphoma						
SD	434.37	0.720	0.778	0.735	0.796	<0.001
$Entropy_{HIST}$	5.22	0.720	0.889	0.765	0.791	0.001
Volume	16,064	0.680	0.889	0.735	0.787	0.001
Area	4016	0.680	0.889	0.735	0.787	0.001
Max-diameter	42.9	0.720	0.778	0.735	0.729	0.014
SUVmax	5.00	0.880	0.889	0.882	0.818	0.001
SUVmean	3.10	0.880	0.889	0.882	0.842	<0.001
Low-grade gastric lymphoma *vs.* gastric cancer						
$Entropy_{GLCM10}$	7.45	0.733	0.778	0.741	0.746	0.004
$Entropy_{GLCM11}$	8.36	0.644	0.889	0.685	0.762	0.001
$Entropy_{GLCM12}$	7.45	0.711	0.778	0.722	0.770	0.001
$Entropy_{GLCM13}$	7.70	0.733	0.778	0.741	0.746	0.005
Volume	16,064.00	0.600	0.889	0.648	0.720	0.019
Area	4016.00	0.600	0.889	0.648	0.720	0.019

ROC: Receiver operating characteristic; SUV: Standard uptake value; SD: Standard deviation; HIST: Histogram; GLCM: Grey-level co-occurrence matrix; AUC: Area under the curve.

ROC analysis

Parameters with significant differences between groups were subjected to ROC analysis. The results are presented in Table 5. In the differentiation of gastric lymphoma and gastric cancer, $inertia_{GLCM}$ had the highest AUC (sensitivity = 0.778, specificity = 0.647, accuracy = 0.722, AUC = 0.714, $P < 0.001$). SUVmax and SUVmean were the most discriminating parameters in differentiating low-grade and high-grade gastric lymphoma (sensitivity = 0.880 and

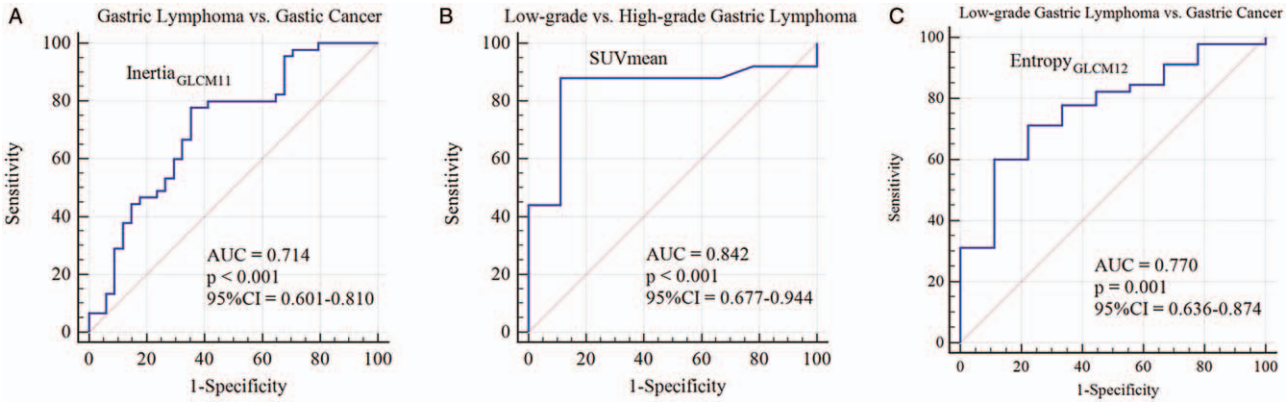

Figure 3: Receiver operating characteristic curves of inertia$_{GLCM11}$ (A), SUVmean (B), and entropy$_{GLCM12}$ (C) in differentiating gastric lymphoma *vs.* gastric cancer, low-grade *vs.* high-grade lymphoma, and low-grade gastric lymphoma *vs.* gastric cancer, respectively. AUC: Area under the curve; CI: Confidence interval; GLCM: Grey-level co-occurrence matrix; SUV: Standard uptake value.

0.880, specificity = 0.889 and 0.889, accuracy = 0.882 and 0.882, AUC = 0.818 and 0.842, $P = 0.001$ and <0.001, respectively). Entropy$_{GLCM}$ had the highest AUC in distinguishing low-grade gastric lymphoma and gastric cancer (sensitivity = 0.711, specificity = 0.778, accuracy = 0.722, AUC = 0.770, $P = 0.001$) [Figure 3].

Intra-observer and inter-observer agreement analysis

Mean, SD, maximum, percentiles (10th, 25th, 50th, 75th, and 90th), kurtosis, entropy, volume, area, max diameter, inertia$_{GLCM10}$, inertia$_{GLCM11}$, inertia$_{GLCM12}$, and inertia$_{GLCM13}$ exhibited excellent intra-observer agreement (the ICCs ranged from 0.827 to 0.999). Max frequency, mode, minimum, 5th percentile, skewness, entropy$_{GLCM10}$, entropy$_{GLCM11}$, entropy$_{GLCM12}$, and entropy$_{GLCM13}$ exhibited good intra-observer agreement (the ICCs ranged from 0.724 to 0.800).

Mean, SD, max frequency, maximum, percentiles (25th, 50th, 75th and 90th), kurtosis, entropy, volume, area, max diameter, entropy$_{GLCM10}$, entropy$_{GLCM11}$, entropy$_{GLCM12}$, entropy$_{GLCM13}$, inertia$_{GLCM10}$, inertia$_{GLCM11}$, inertia$_{GLCM12}$, and inertia$_{GLCM13}$ exhibited excellent interobserver agreement (the ICCs ranged from 0.801 to 0.998). Mode, minimum, 5th percentile, 10th percentile, and skewness exhibited good interobserver agreement (the ICCs ranged from 0.717 to 0.800). The details of the ICCs are provided in Supplemental Tables 1 and 2, http://links.lww.com/CM9/A377.

Discussion

The present study explored the role of PET TA in differentiating gastric lymphoma *vs.* gastric cancer, low-grade gastric lymphoma *vs.* high-grade gastric lymphoma, and low-grade gastric lymphoma *vs.* gastric cancer. The differential efficacies of the texture features were compared with those of traditional SUVs.

SUVs, grey-level intensity features, percentiles and inertia$_{GLCM}$ were discriminating features in differentiating gastric lymphoma from gastric cancer, and inertia$_{GLCM11}$ had the highest AUC among these features. However, no significant differences in the FDG uptake level existed between low-grade lymphoma and gastric cancer, while the texture feature entropy$_{GLCM}$ exhibited good efficacy in differentiating low-grade lymphoma and gastric cancer.

SUVmax and SUVmean are the commonly used semi-quantitative parameters in daily ^{18}F-FDG PET scans. They represent the degree of FDG uptake in ROIs, which depends on glucose transporter (GLUT) expression and hexokinase activity. In general, SUVs are lower in gastric cancer due to the lower expression of GLUT-1 transporters, a decrease in cellular density, and an increase in intracellular mucin.[28] However, low-grade lymphoma, such as gastric MALT lymphoma, was found to have low FDG avidity, thus usually had relatively low SUVs.[19] In the present study, the SUVs were not significantly different between low-grade gastric lymphoma and gastric cancer. Thus, it remains difficult to differentiate these malignancies when relying on these routinely used semiquantitative parameters.

The maximum, minimum, mean, and percentiles describe the distribution of grey-level intensities in an ROI. FDG uptake is transferred to grey-level intensity in PET images. The higher the radioactivity counts one pixel has, the higher the grey-level intensity it presents. Similar to SUVs, grey-level intensity parameters actually reflect the degree of FDG uptake in PET images, resulting in the substantial correlation between these parameters and SUVs, as well as the similar efficacy in the differentiation of gastric cancer and gastric lymphoma.

Inertia describes the variation in local grey-level intensity values between a pixel and its neighbors.[29] In a GLCM, the element $G(i, j)$ is the sum of the number of times that the pixel with grey-level intensity value i occurs in the specified spatial relationship (with a given distance and on a given direction) to a pixel with a grey-level intensity value j in the input image.[30] Inertia$_{GLCM}$ is defined by the formula, $Inertia = \sum i,j(I-j)^2 G(i, j)$. The greater the difference is between value i and j, the higher the inertia$_{GLCM}$ becomes. The importance of inertia in differential diagnosis and

prognosis has been demonstrated by several studies.[29,31,32] In the present study, $inertia_{GLCM}$ was found to be higher in gastric lymphoma than that in gastric cancer on all four directions in the cross-sectional PET image (that is $inertia_{GLCM10}$, $inertia_{GLCM11}$, $inertia_{GLCM12}$, and $inertia_{GLCM13}$), making it capable of differentiating gastric lymphoma from gastric cancer with AUCs (0.688–0.714) higher than those of all other parameters being analyzed. These results suggest that the local FDG uptake variation was significantly higher in gastric lymphoma, which could be important in differentiating gastric lymphoma from gastric cancer. Although the cause of this characterization was unclear, the investigators hypothesized that this could be attributed to regional tissues with extremely higher FDG uptake than the surroundings in gastric lymphoma. Notably, the specificity of $inertia_{GLCM11}$ was higher than that of SUVmax and SUVmean (0.647 *vs.* 0.382 and 0.441, respectively). Since gastric lymphoma was set to be "negative" in the ROC analysis, this suggested that $inertia_{GLCM11}$ was more capable than SUVs in differentiating gastric lymphoma from gastric cancer.

Entropy quantitatively characterizes intra-tumor heterogeneity. Histogram entropy describes the distribution of grey-level intensities inside the ROI, and second-order entropies (such as $entropy_{GLCM}$) provide information on the positional relationship between groups of two pixels.[33] The more chaotic the image is, the higher the entropy would be. Low-grade lymphoma lesions tend to be comprised of aligned monomorphic lymphoid cells. Thus, these can be characterized as more homogeneous in medical images, which generates lower entropies. In the present study, $entropy_{GLCM}$ was found to be significantly lower in the low-grade gastric lymphoma group. This allows it to be able to discriminate low-grade gastric lymphoma and gastric cancer, and it was superior to SUVs and other texture features.

Kurtosis and skewness, describe the sharpness of the peak and asymmetry of the grey-level intensity distribution, respectively. However, these were found to have no significant differences among the groups. The grey-level intensity distributions of both groups were leptokurtic right-skewed. The kurtosis and skewness in PET TA varied according to the objects of study. In a study that included 40 uterine leiomyoma patients and 15 uterine sarcoma patients, kurtosis and skewness were significantly higher in uterine sarcoma.[34] Although the authors did not provide a clear explanation, we considered that a possible reason is that the FDG uptake in uterine sarcoma is significantly higher than that in leiomyoma, resulting in extremely higher grey-level intensity values in uterine sarcoma. Another PET TA of 50 patients with thyroid incidentaloma revealed that the skewness of thyroid malignancies was significantly lower than that of benign nodules, while kurtosis was not significantly different between groups.[35] In contrast, kurtosis and skewness were found to have no significant differences between the baseline and intra-treatment PET images in patients with non-small cell lung cancer.[36] In PET TA, due to the diversity of the tumor biological characteristics, especially the diversity of cellular FDG uptake, the application value of kurtosis and skewness fluctuates according to the tumor being studied.

The present study had some limitations. First, this was a preliminary retrospective study, and all the hypotheses were only supported by statistical analysis. Due to the limited cohort size, it was not reliable enough to generate a regression model for the differential diagnosis. Thus, it is important to validate these results with enlarged sample size or a prospective study in the future. Second, diffuse or focal increased FDG uptake could be observed in normal gastric walls. To avoid this pitfall, the gastric wall thickness in the hybrid CT images and positional information from the pathologic examination were taken into consideration during the ROI delineation. The ICC analysis also confirmed the reliability of the present results. Third, considering the heterogeneous FDG uptake in the different subtypes of lymphoma, the investigators roughly divided the gastric lymphoma cases into low-grade and high-grade gastric lymphoma groups. Hence, there could still be potential differences due to the variety of pathological subtypes (such as T-cell lymphoma *vs.* B-cell lymphoma). In addition, the gastric cancer cases were not divided into subgroups based on histological subtypes, since the FDG avidity of different subtypes of gastric cancer is not as heterogeneous as that of gastric lymphoma. Further studies will be performed to explore the use of PET TA in gastric cancer and gastric lymphoma with unified pathological subtypes.

In conclusion, $inertia_{GLCM}$ was the most discriminating feature in differentiating gastric lymphoma from gastric cancer, and $entropy_{GLCM}$ could differentiate between low-grade gastric lymphoma and gastric cancer. PET TA could serve as a promising non-invasive tool for improving the differential diagnosis of gastric neoplasms, especially for tumors with a similar degree of FDG uptake.

Conflicts of interest

None.

References

1. Siegel RL, Miller KD, Jemal A. Cancer statistics, 2019. CA Cancer J Clin 2019;69:7–34. doi: 10.3322/caac.21551.
2. Juarez-Salcedo LM, Sokol L, Chavez JC, Dalia S. Primary gastric lymphoma, epidemiology, clinical diagnosis, and treatment. Cancer Control 2018;25:1073274818778256. doi: 10.1177/1073274818778256.
3. Ikoma N, Badgwell BD, Mansfield PF. Multimodality treatment of gastric lymphoma. Surg Clin North Am 2017;97:405–420. doi: 10.1016/j.suc.2016.11.012.
4. Ishikawa E, Nakamura M, Shimada K, Tanaka T, Satou A, Kohno K, *et al*. Prognostic impact of PD-L1 expression in primary gastric and intestinal diffuse large B-cell lymphoma. J Gastroenterol 2020;55:39–50. doi: 10.1007/s00535-019-01616-3.
5. Martin-Richard M, Carmona-Bayonas A, Custodio AB, Gallego J, Jimenez-Fonseca P, Reina JJ, *et al*. SEOM clinical guideline for the diagnosis and treatment of gastric cancer (GC) and gastroesophageal junction adenocarcinoma (GEJA) (2019). Clin Transl Oncol 2020;22:236–244. doi: 10.1007/s12094-019-02259-9.
6. Lott PC, Carvajal-Carmona LG. Resolving gastric cancer aetiology: an update in genetic predisposition. Lancet Gastroenterol Hepatol 2018;3:874–883. doi: 10.1016/s2468-1253(18)30237-1.
7. Noh CK, Jung MW, Shin SJ, Ahn JY, Cho HJ, Yang MJ, *et al*. Analysis of endoscopic features for histologic discrepancies between biopsy and endoscopic submucosal dissection in gastric neoplasms: 10-year results. Dig Liver Dis 2019;51:79–85. doi: 10.1016/j.dld.2018.08.027.

8. Xu G, Zhang W, Lv Y, Zhang B, Sun Q, Ling T, *et al*. Risk factors for under-diagnosis of gastric intraepithelial neoplasia and early gastric carcinoma in endoscopic forceps biopsy in comparison with endoscopic submucosal dissection in Chinese patients. Surg Endosc 2016;30:2716–2722. doi: 10.1007/s00464-015-4534-x.
9. Li R, Li J, Wang X, Liang P, Gao J. Detection of gastric cancer and its histological type based on iodine concentration in spectral CT. Cancer Imaging 2018;18:42. doi: 10.1186/s40644-018-0176-2.
10. Liu S, Shi H, Ji C, Zheng H, Pan X, Guan W, *et al*. Preoperative CT texture analysis of gastric cancer: correlations with postoperative TNM staging. Clin Radiol 2018;73:756.e1–756.e9. doi: 10.1016/j.crad.2018.03.005.
11. Ma Z, Fang M, Huang Y, He L, Chen X, Liang C, *et al*. CT-based radiomics signature for differentiating Borrmann type IV gastric cancer from primary gastric lymphoma. Eur J Radiol 2017;91:142–147. doi: 10.1016/j.ejrad.2017.04.007.
12. Cai JS, Chen HY, Chen JY, Lu YF, Sun JZ, Zhou Y, *et al*. Reduced field-of-view diffusion-weighted imaging (DWI) in patients with gastric cancer: comparison with conventional DWI techniques at 3.0T: a preliminary study. Medicine (Baltimore) 2020;99:e18616. doi: 10.1097/MD.0000000000018616.
13. Avcu S, Arslan H, Unal O, Kotan C, Izmirli M. The role of diffusion-weighted MR imaging and adc values in the diagnosis of gastric tumors. JBR-BTR 2012;95:1–5. doi: 10.5334/jbr-btr.62.
14. Marcus C, Subramaniam RM. PET/computed tomography and precision medicine: gastric cancer. PET Clin 2017;12:437–447. doi: 10.1016/j.cpet.2017.05.004.
15. Chen R, Chen Y, Huang G, Liu J. Relationship between PD-L1 expression and 18F-FDG uptake in gastric cancer. Aging (Albany NY) 2019;11:12270–12277. doi: 10.18632/aging.102567.
16. Zhou Y, Ma XL, Pu LT, Zhou RF, Ou XJ, Tian R. Prediction of overall survival and progression-free survival by the (18)F-FDG PET/CT radiomic features in patients with primary gastric diffuse large B-cell lymphoma. Contrast Media Mol Imaging 2019;2019:5963607. doi: 10.1155/2019/5963607.
17. Li XF, Fu Q, Dong YW, Liu JJ, Song XY, Dai D, *et al*. (18)F-fluorodeoxyglucose positron emission tomography/computed tomography comparison of gastric lymphoma and gastric carcinoma. World J Gastroenterol 2016;22:7787–7796. doi: 10.3748/wjg.v22.i34.7787.
18. Mehdikhani H, Heiba S. Successful staging of synchronous gastric cancer and diffuse large B-cell lymphoma (Dlbcl) using F-18-fluorodeoxyglucose positron emission tomography/computed tomography (FDG PET/CT) based on distinctive levels of metabolic activity between the two malignancies. Indian J Nucl Med 2017;32:85–86. doi: 10.4103/0972-3919.198517.
19. Albano D, Bertoli M, Ferro P, Fallanca F, Gianolli L, Picchio M, *et al*. 18F-FDG PET/CT in gastric MALT lymphoma: a bicentric experience. Eur J Nucl Med Mol Imaging 2017;44:589–597. doi: 10.1007/s00259-016-3518-y.
20. Hatt M, Tixier F, Pierce L, Kinahan PE, Le Rest CC, Visvikis D. Characterization of PET/CT images using texture analysis: the past, the present... any future? Eur J Nucl Med Mol Imaging 2017;44:151–165. doi: 10.1007/s00259-016-3427-0.
21. Lippi M, Gianotti S, Fama A, Casali M, Barbolini E, Ferrari A, *et al*. Texture analysis and multiple-instance learning for the classification of malignant lymphomas. Comput Methods Programs Biomed 2019;185:105153. doi: 10.1016/j.cmpb.2019.105153.
22. Buvat I, Orlhac F, Soussan M. Tumor texture analysis in PET: where do we stand? J Nucl Med 2015;56:1642–1644. doi: 10.2967/jnumed.115.163469.
23. Chicklore S, Goh V, Siddique M, Roy A, Marsden PK, Cook GJ. Quantifying tumour heterogeneity in 18F-FDG PET/CT imaging by texture analysis. Eur J Nucl Med Mol Imaging 2013;40:133–140. doi: 10.1007/s00259-012-2247-0.
24. Liu S, Shi H, Ji C, Guan W, Chen L, Sun Y, *et al*. CT textural analysis of gastric cancer: correlations with immunohistochemical biomarkers. Sci Rep 2018;8:11844. doi: 10.1038/s41598-018-30352-6.
25. Wang Y, Jin ZY. Radiomics approaches in gastric cancer: a frontier in clinical decision making. Chin Med J 2019;132:1983–1989. doi: 10.1097/CM9.0000000000000360.
26. Krarup MMK, Nygard L, Vogelius IR, Andersen FL, Cook G, Goh V, *et al*. Heterogeneity in tumours: validating the use of radiomic features on (18)F-FDG PET/CT scans of lung cancer patients as a prognostic tool. Radiother Oncol 2019;144:72–78. doi: 10.1016/j.radonc.2019.10.012.
27. Lue KH, Wu YF, Liu SH, Hsieh TC, Chuang KS, Lin HH, *et al*. Intratumor heterogeneity assessed by (18)F-FDG PET/CT predicts treatment response and survival outcomes in patients with Hodgkin lymphoma. Acad Radiol 2020;27:e183–e192. doi: 10.1016/j.acra.2019.10.015.
28. Malibari N, Hickeson M, Lisbona R. PET/computed tomography in the diagnosis and staging of gastric cancers. PET Clin 2015;10:311–326. doi: 10.1016/j.cpet.2015.03.008.
29. Tan S, Kligerman S, Chen W, Lu M, Kim G, Feigenberg S, *et al*. Spatial-temporal [(1)(8)F]FDG-PET features for predicting pathologic response of esophageal cancer to neoadjuvant chemoradiation therapy. Int J Radiat Oncol Biol Phys 2013;85:1375–1382. doi: 10.1016/j.ijrobp.2012.10.017.
30. Zulpe NPV. GLCM texture features for Brain tumor Classification. Int J Comp Sci Iss 2012;9:354–359.
31. Wang H, Guo XH, Jia ZW, Li HK, Liang ZG, Li KC, *et al*. Multilevel binomial logistic prediction model for malignant pulmonary nodules based on texture features of CT image. Eur J Radiol 2010;74:124–129. doi: 10.1016/j.ejrad.2009.01.024.
32. Mattonen SA, Palma DA, Haasbeek CJ, Senan S, Ward AD. Early prediction of tumor recurrence based on CT texture changes after stereotactic ablative radiotherapy (SABR) for lung cancer. Med Phys 2014;41:033502. doi: 10.1118/1.4866219.
33. Liu S, Zheng H, Zhang Y, Chen L, Guan W, Guan Y, *et al*. Whole-volume apparent diffusion coefficient-based entropy parameters for assessment of gastric cancer aggressiveness. J Magn Reson Imaging 2018;47:168–175. doi: 10.1002/jmri.25752.
34. Tsujikawa T, Yamamoto M, Shono K, Yamada S, Tsuyoshi H, Kiyono Y, *et al*. Assessment of intratumor heterogeneity in mesenchymal uterine tumor by an (18)F-FDG PET/CT texture analysis. Ann Nucl Med 2017;31:752–757. doi: 10.1007/s12149-017-1208-x.
35. Sollini M, Cozzi L, Pepe G, Antunovic L, Lania A, Di Tommaso L, *et al*. [(18)F]FDG-PET/CT texture analysis in thyroid incidentalomas: preliminary results. Eur J Hybrid Imaging 2017;1:3. doi: 10.1186/s41824-017-0009-8.
36. Dong X, Sun X, Sun L, Maxim PG, Xing L, Huang Y, *et al*. Early change in metabolic tumor heterogeneity during chemoradiotherapy and its prognostic value for patients with locally advanced non-small cell lung cancer. PloS One 2016;11:e0157836. doi: 10.1371/journal.pone.0157836.

How to cite this article: Sun YW, Ji CF, Wang H, He J, Liu S, Ge Y, Zhou ZY. Differentiating gastric cancer and gastric lymphoma using texture analysis (TA) of positron emission tomography (PET). Chin Med J 2021;134:439–447. doi: 10.1097/CM9.0000000000001206